Revisiting Mismatch Uncertainty with the Rayleigh Distribution

White Paper

Abstract—*This paper examines several important aspects of estimating mismatch uncertainty, which is often a major component of the total uncertainty for RF and microwave measurements. Expressions for mismatch correction and the corresponding uncertainty are presented for reflection coefficients with known magnitude and phase. For reflection coefficients with unknown phase, two scenarios are considered; that is, when estimates exist for the reflection coefficient magnitude resulting in the well-known U-shaped uncertainty distribution and when dealing with assumed reflection coefficient magnitude values. For the latter scenario, this paper demonstrates that the reflection coefficient magnitude is best modeled with a Rayleigh distribution. Measurement data is presented revealing a very good fit to the Rayleigh distribution. Finally, this paper presents methods for estimating the Rayleigh distribution parameter from information found in manufacturer's data sheets. The objective of this paper is to provide comprehensive techniques for estimating realistic mismatch uncertainty, which usually gives a three to six times lower estimate of mismatch uncertainty compared with estimates from commonly used techniques.*

Speaker/Author: Michael Dobbert
Agilent Technologies
1400 Fountaingrove Parkway, Mail Stop: 3USH, Santa Rosa, CA 95403
E-mail: dobbert-metrology@agilent.com

Co-Author: Joe Gorin
Agilent Technologies
1400 Fountaingrove Parkway, Mail Stop: 4UST, Santa Rosa, CA 95403
E-mail: gorin_signal_analysis@agilent.com

Introduction

Mismatch affects the accuracy of measurements made using RF and microwave equipment such as power meters, signal analyzers, noise figure meters, network analyzers, high frequency oscilloscopes, signal generators, attenuators, couplers, cables and adapters. The measurement uncertainty due to mismatch is often a major component of the total uncertainty for RF and microwave measurements.

For RF and microwave systems, knowledge of the complex-valued quantities of source and load reflection coefficients allows for correcting for mismatch with a corresponding uncertainty. However, for many measurements, only reflection coefficient magnitude is known. The lack of phase information precludes the ability to correct for mismatch and is a source of measurement error when making power measurements. The distribution of errors due to mismatch when dealing with unknown phase is often associated with the well-known U-shaped probability distribution. However, this component of uncertainty is only part of the picture. The total mismatch uncertainty must also consider the errors associated with reflection coefficient magnitude. The total uncertainty may be determined by using an estimate and an associated uncertainty, or by assigning a probability density function (PDF) to the reflection coefficient magnitude. This paper demonstrates both.

Assigning a probability density function to the reflection coefficient magnitude finds its use when reflection coefficient magnitude data is available from a manufacturer's data sheet or a pooled data set. The natural tendency is for reflection coefficient magnitude to take on a Rayleigh probability distribution. This paper gives several methods for estimating the Rayleigh distribution parameter from available data enabling the estimation of mismatch uncertainty.

2. Mismatch

Mismatch is the term used to describe the consequence of traveling waves that reflect off the various structures within RF and microwave transmission systems.

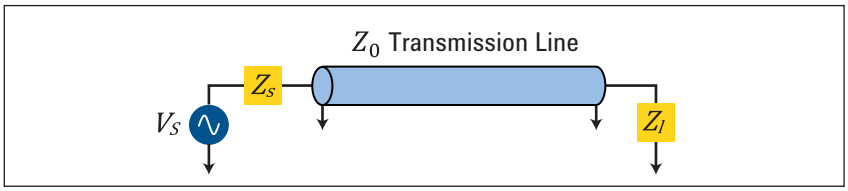

Figure 1. A generator connected to a load through a transmission line.

Consider a signal generator with output impedance Z_s, connected to a load, Z_l, through a lossless transmission line with characteristic impedance Z_0, as shown in Figure 1. Of interest with this circuit are the forward and reverse traveling voltage waves on the transmission line. From the generator, a traveling voltage wave moves along the transmission line towards the load. If the load impedance does not exactly match the characteristic impedance of the transmission line, a second traveling voltage wave reflected off the load heads back towards the generator. The magnitude of this reflected, reverse traveling wave depends on the load impedance. For many microwave power measurements, the magnitude of the reflected wave is small, ideally, relative to the forward wave. The reverse traveling voltage wave, upon reaching the generator, re-reflects back in the forward direction adding to the traveling voltage wave from the generator. The magnitude of the re-reflected voltage wave depends on the generator impedance. The voltage wave from the generator and the re-reflected voltage wave add either constructively or destructively, depending upon the relative phase of the two traveling waves. The net magnitude of the forward and reverse traveling voltage waves are the result of multiple reflections and rereflections. In a system such as this, the voltage at the load depends on the load impedance, the impedance of the generator and propagation delay of the transmission line.

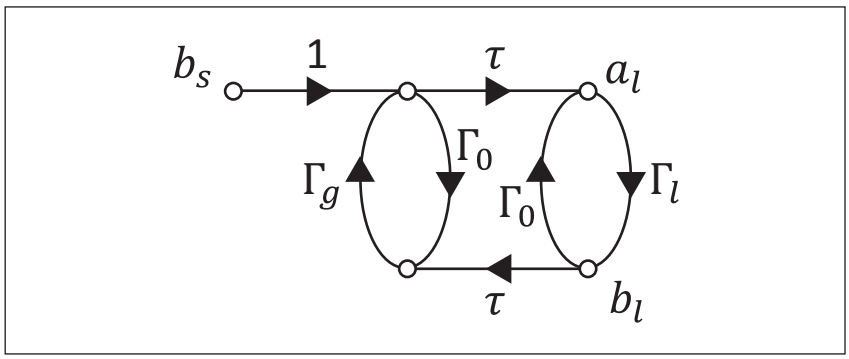

Figure 2. Flow diagram for Figure 1.

The flow diagram in Figure 2 models the circuit from Figure 1 where,

- b_s = traveling voltage wave produced by the generator,
- a_l = traveling voltage wave incident on the load,
- b_l = traveling voltage wave reflected off the load,
- Γ_g = generator reflection coefficient where $\Gamma_s = \frac{Z_s - Z_0}{Z_s + Z_0}$,
- Γ_l = load reflection coefficient where $\Gamma_l = \frac{Z_l - Z_0}{Z_l + Z_0}$,
- τ = transmission coefficient of the transmission line,
- Γ_0 = input and output reflection coefficient of the transmission line.

The transmission line, in this circuit, is assumed lossless and otherwise ideal, such that $\Gamma_0 = \frac{Z_0 - Z_0}{Z_0 + Z_0} = 0$ and $|\tau| = 1$. In addition, the effect of the transmission line propagation delay simply offsets the phase of Γ_l as seen at the generator. As such, assuming constant phase for τ has no impact on the remaining analysis, but along with assuming $\Gamma_0 = 0$, allows for a simplification of the circuit model as shown in Figure 3.

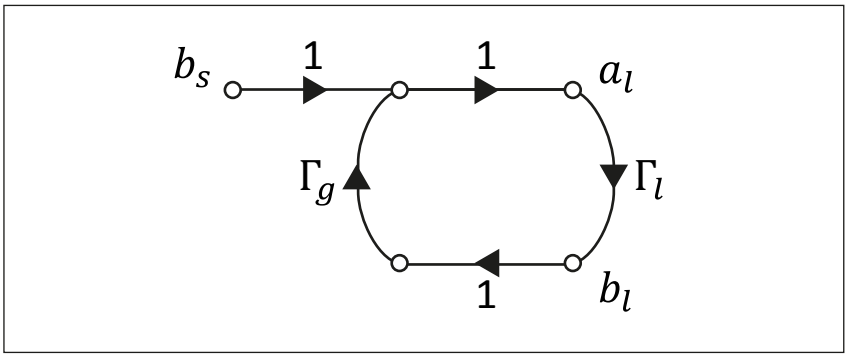

Figure 3. Simplified circuit model.

Relying on Mason's non-touching loop rule for signal flow graphs

$$a_l = \frac{b_s}{1 - \Gamma_l \Gamma_g} \qquad \textit{Equation 1}$$

$$b_l = \frac{b_s \Gamma_l}{1 - \Gamma_l \Gamma_g} \qquad \textit{Equation 2}$$

The power absorbed by the load, P_a, is the difference between the power incident upon the load and the power reflected off the load.

$$P_a = |a_l|^2 - |b_l|^2 = |b_s|^2 \frac{1 - |\Gamma_l|^2}{|1 - \Gamma_l \Gamma_g|^2} \qquad \textit{Equation 3}$$

When the load impedance equals the characteristic impedance, then $\Gamma_l = 0$, and

$$P_a\big|_{\Gamma_l=0} = |b_s|^2 = P_{gZ0} \qquad \textit{Equation 4}$$

P_{gZ0} represents the power the generator delivers to a perfectly matched load. The power absorbed by a load of arbitrary impedance is related to the power a generator delivers to a perfectly matched load, and the impedances of the actual load and the generator.

$$P_a = P_{gZ0}\frac{1-|\Gamma_l|^2}{|1-\Gamma_l\Gamma_g|^2} \qquad \textit{Equation 5}$$

The term $1-|\Gamma_l|^2$, in equation (5) represents mismatch loss. Mismatch loss is solely a function of the load impedance. That is, load impedance not equal to the characteristic impedance reduces the absorbed power relative to the power absorbed by a perfectly matched load. For powermeasuring devices such as a power meter or a signal analyzer, calibration corrects for the mismatch loss of these devices. For example, the power sensor correction factor applied to power measurements, using a power meter, corrects for all known systematic errors of the power sensor, including mismatch loss.

Whereas the calibration of a power measuring device generally accounts for mismatch loss, accounting for the term $|1-\Gamma_l\Gamma_g|^2$, which represents the effect of multiple reflections, requires knowledge of both Γ_l and Γ_g. Γ_l and Γ_g are complex quantities; evaluating $|1-\Gamma_l\Gamma_g|^2$ and correcting for multiple reflections in power measurements is straightforward. The uncertainty associated with $|1-\Gamma_l\Gamma_g|^2$ is determined from the uncertainty of the estimates of Γ_l and Γ_g. Defining the quantity M,

$$M = |1-\Gamma_l\Gamma_g|^2 \qquad \textit{Equation 6}$$

where $\Gamma_l = \Gamma_{l.re} + i\Gamma_{l.im}$ and $\Gamma_g = \Gamma_{g.re} + i\Gamma_{g.im}$ representing the real and imaginary components of Γ_l and Γ_g. Then

$$M = \left|1-\left(\Gamma_{l.re}\Gamma_{g.re} - \Gamma_{l.im}\Gamma_{g.im}\right) - i\left(\Gamma_{l.re}\Gamma_{g.im} + \Gamma_{l.im}\Gamma_{g.re}\right)\right|^2 \qquad \textit{Equation 7}$$

Letting $R = \left(1-\Gamma_{l.re}\Gamma_{g.re} + \Gamma_{l.im}\Gamma_{g.im}\right)$ and $I = -\left(\Gamma_{l.re}\Gamma_{g.im} + \Gamma_{l.im}\Gamma_{g.re}\right)$, the sensitivity coefficients, as per the GUM [1], are

$$c_{l.re} = \frac{\partial M}{\partial \Gamma_{l.re}} = -2\left(\Gamma_{g.re}R + \Gamma_{g.im}I\right) \qquad \textit{Equation 8}$$

$$c_{l.im} = \frac{\partial M}{\partial \Gamma_{l.im}} = 2\left(\Gamma_{g.im}R - \Gamma_{g.re}I\right) \qquad \textit{Equation 9}$$

$$c_{g.re} = \frac{\partial M}{\partial \Gamma_{g.re}} = -2\left(\Gamma_{l.re}R + \Gamma_{l.im}I\right) \qquad \textit{Equation 10}$$

$$c_{g.im} = \frac{\partial M}{\partial \Gamma_{g.im}} = 2\left(\Gamma_{l.im}R - \Gamma_{l.re}I\right) \qquad \textit{Equation 11}$$

Often, Γ_l and Γ_g are uncorrelated. However, in general, the real and imaginary parts of Γ_l and the real and imaginary parts of Γ_g are correlated. This leads to an uncertainty equation for M as,

$$u(M) = \sqrt{\begin{array}{c}\left[c_{l.re}u\left(\Gamma_{l.re}\right)\right]^2 + \left[c_{l.im}u\left(\Gamma_{l.im}\right)\right]^2 + \left[c_{g.re}u\left(\Gamma_{g.re}\right)\right]^2 + \left[c_{g.im}u\left(\Gamma_{g.im}\right)\right]^2 \\ +2c_{l.re}c_{l.im}u\left(\Gamma_{l.re},\Gamma_{l.im}\right) + 2c_{g.re}c_{g.im}u\left(\Gamma_{g.re},\Gamma_{g.im}\right)\end{array}} \qquad \textit{Equation 12}$$

Equation (12) requires estimates of the real and imaginary components of reflection coefficient and associated uncertainty and covariance. Often, however, reflection coefficient is reported as magnitude and phase. Appendix A gives an expression for transforming reflection coefficient uncertainties as magnitude and phase to real and imaginary representation.

3. Unknown Phase

Obtaining phase information for both Γ_l and Γ_g is often non-trivial, especially for signal generators. Traditional reflection coefficient measurements using a vector network analyzer may not be feasible due to the signal generator's own signal output. Therefore, reflection coefficient magnitude may be known, but not reflection coefficient phase for either Γ_l or Γ_g, or both. It is reasonable to assume that phase can take on any value in the range $-\pi < \varphi \leq \pi$. Furthermore, any value of phase is equally likely. This leads to possible values of reflection coefficient with circular symmetry about the origin of the real-imaginary plane. Note however, that when determining measurement uncertainty involving complex reflection coefficient quantities, it is desirable to express uncertainty as real and imaginary components. Doing so allows for determining uncertainty involving complex values that is consistent with the GUM (see Ridler and Salter [2]) and it avoids nonlinearity issues with the transformation between rectangular and polar coordinates when reflection coefficient values are near the origin.

Given circular symmetry about the origin, the real and imaginary reflection coefficient uncertainties are equal. Additionally, the best estimate for the real and imaginary parts of reflection coefficient is zero. This presents a problem when determining uncertainty. Examination of equations (8) through (11) reveals that the sensitivity coefficients are all zero when this is the case. Hall [3][4] has addressed this. That is, let $G = \Gamma_l\Gamma_g$ so that

$$M = \left|1 - G\right|^2 \qquad \textit{Equation 13}$$

and

$$M = \left(1 - G_{re}\right)^2 + \left(-G_{im}\right)^2 \qquad \textit{Equation 14}$$

where G_{re} and G_{im} are the real and imaginary components of G, respectively. The sensitivity coefficients are

$$c_{re} = \frac{\partial M}{\partial G_{re}} = -2\left(1 - G_{re}\right) \quad \textit{Equation 15}$$

$$c_{im} = \frac{\partial M}{\partial G_{im}} = 2G_{im} \quad \textit{Equation 16}$$

Assuming the best estimate of G_{re} and G_{im} is zero, then $c_{re} = 2$, $c_{im} = 0$ and

$$u\left(M\right) = \sqrt{2^2 u^2\left(G_{re}\right)} = 2u\left(G_{re}\right) \quad \textit{Equation 17}$$

Even though the real and imaginary uncertainties are equal, given the circular symmetry assumption, equation (17) shows that the uncertainty due mismatch only depends on $u\left(G_{re}\right)$ is the product of Γ_l and Γ_g, and in the case of unknown phase, the uncertainty of G_{re} is (see [3]),

$$u\left(G_{re}\right) = \sqrt{2}u\left(\Gamma_{l.re}\right)u\left(\Gamma_{g.re}\right) \quad \textit{Equation 18}$$

Combining equations (17) and (18),

$$u\left(M\right) = 2\sqrt{2}u\left(\Gamma_{l.re}\right)u\left(\Gamma_{g.re}\right) \quad \textit{Equation 19}$$

Equation (19) shows that the uncertainty due to mismatch when phase is not known can be determined from the real components of the corresponding reflection coefficient uncertainties. Note that the uncertainty due to mismatch can also be determined from the imaginary components since the real and imaginary components are equal in this case.

For the moment, assuming known constant values for $\left|\Gamma_l\right|$ or $\left|\Gamma_g\right|$, with unknown, but equally likely phase values over the range of range $-\pi < \varphi \le \pi$, the range of possible reflection coefficient values lie on a circle centered on the origin of the real and imaginary plane. The standard deviation of the real component of reflection coefficient, in this case is

$$\sigma = \frac{a}{\sqrt{2}} \quad \textit{Equation 20}$$

where a is the circle radius. This is the result given by Harris and Warner [5]. The distribution of possible values is what Harris and Warner referred to as **U**-shaped. Letting $a = \left|\Gamma_l\right|$, and also $a = \left|\Gamma_g\right|$, the standard uncertainty of the real component of for Γ_l and Γ_g are

$$u\left(\Gamma_{l.re}\right) = \frac{\left|\Gamma_l\right|}{\sqrt{2}} \quad \textit{Equation 21}$$

$$u\left(\Gamma_{g.re}\right) = \frac{\left|\Gamma_g\right|}{\sqrt{2}} \quad \textit{Equation 22}$$

Given equation (19), the uncertainty of M, when assuming known magnitude values of reflection coefficient and unknown phase, is,

$$u(M) = 2\sqrt{2}\frac{|\Gamma_l|}{\sqrt{2}}\frac{|\Gamma_g|}{\sqrt{2}} = \sqrt{2}|\Gamma_l||\Gamma_g| \qquad \textit{Equation 23}$$

Equation (23) assumes complete knowledge of $|\Gamma_l|$ and $|\Gamma_g|$. However, if $|\Gamma_l|$ and $|\Gamma_g|$ are the results of measurements, then error exists with the estimate of $|\Gamma_l|$ and $|\Gamma_g|$. If this error is small, then the errors due to unknown phase information dominate the uncertainty of M. If this is the case, then equation (23) provides a reasonable estimate for the uncertainty of M.

4. Measured Values for $|\Gamma_l|$ and $|\Gamma_g|$

If Γ_l and Γ_g are measured quantities, with a corresponding uncertainty yet with unknown phase, the distribution of possible reflection coefficient values lie within an annulus-like shaped region centered on the origin of the real and imaginary plane. The uncertainty of Γ_l and Γ_g with this distribution shape is (see [4]),

$$u(\Gamma_{l.re}) = \frac{1}{\sqrt{2}}\sqrt{|\Gamma_l|^2 + 2u^2(|\Gamma_l|)} \qquad \textit{Equation 24}$$

$$u(\Gamma_{g.re}) = \frac{1}{\sqrt{2}}\sqrt{|\Gamma_g|^2 + 2u^2(|\Gamma_g|)} \qquad \textit{Equation 25}$$

This is the same result assuming the distribution of values within the annulus is uniform, where the inner radius is $a - \sqrt{2}u(a)$ and outer radius is $a + \sqrt{2}u(a)$ and a represents the reflection coefficient magnitude. The uncertainty of M, when relying on measured values of reflection coefficient magnitude is, given equation (19),

$$u(M) = \sqrt{2}\sqrt{|\Gamma_l|^2 + 2u^2(|\Gamma_l|)}\sqrt{|\Gamma_g|^2 + 2u^2(|\Gamma_g|)} \qquad \textit{Equation 26}$$

As the uncertainty of the reflection coefficient magnitude increases relative to the measured value, the distribution of M becomes less and less **U**-shaped (see Figure 4).

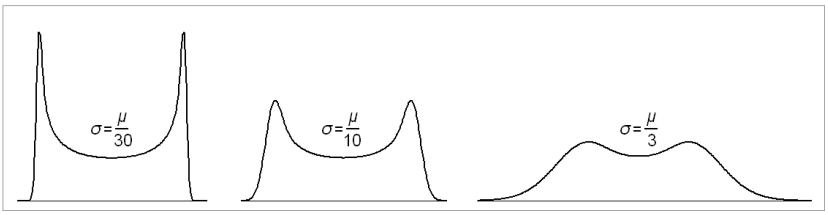

Figure 4. Probability density functions of M.

5. Assumed Rayleigh Distribution for both $|\Gamma_l|$ and $|\Gamma_g|$

Up to this point, the analysis of the uncertainty of M deals with measured values for $|\Gamma_l|$ and $|\Gamma_g|$. Often, however, measured values for $|\Gamma_l|$ and $|\Gamma_g|$ are not available. For example, the calibration of a device may not include reflection coefficient measurements due to the potential difficulty of making the measurements coupled with the general stability of reflection coefficient. In situations such as these, the distribution for $|\Gamma_l|$ and $|\Gamma_g|$ must be assumed. The best information available for reflection coefficient may be the manufacturer's specification, and for many devices, the specification covers a range of frequencies. Unlike a specification that covers the accuracy of a parameter, reflection coefficient specifications are one-sided. That is, reflection coefficient specifications set an upper limit.

For most devices, the mechanical layout and the terminating circuit elements determine reflection coefficient. For example, construction of a typical high frequency, thermocouple power sensor includes a coaxial connector, with a mating surface and mechanical support structure, and a transition to the circuit assembly, which includes a microstrip transmission line and the thermal sensing circuitry. The sensing circuitry typically utilizes a precision thin-film resistor for converting the high frequency energy to heat. Due to the mechanics of the assembly, the transmission path between the terminating thin-film resistor and the mating surface of the input connector includes many small electrical discontinuities, all of which affect the reflection coefficient as measured at the power sensor input. A power sensor has a minimal number of mechanical structures, yet the number of electrical discontinuities on the transmission path adds up quickly.

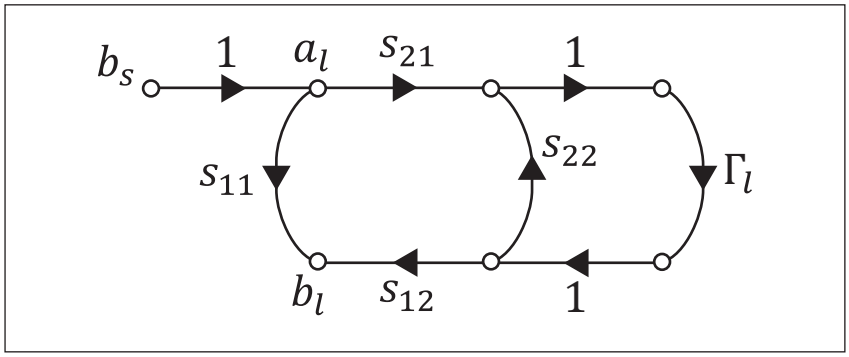

Figure 5. Single discontinuity as a two-port element.

Figure 5 models a single discontinuity as a two-port element, located in front of the terminating circuit element (e.g., the thin-film resistor in the power sensor example). The equivalent impedance of the terminating impedance and the discontinuity is

$$\Gamma_{eq} = \frac{b_l}{a_l} \qquad \textit{Equation 27}$$

Relying on Mason's non-touching loop rule

$$a_l = \frac{b_s}{1-\Gamma_l s_{22}} \qquad \textit{Equation 28}$$

$$b_l = \frac{b_s s_{11}}{1-\Gamma_l s_{22}} + b_s s_{21}\Gamma_l s_{12} \qquad \textit{Equation 29}$$

Combining equations (27), (28) and (29),

$$\Gamma_{eq} = s_{11} + \frac{s_{21}\Gamma_l s_{12}}{1-\Gamma_l s_{22}} \qquad \textit{Equation 30}$$

If the discontinuities are small changes in the transmission line characteristic impedance, then it is safe to assume that $s_{21} = s_{12} = 1$. This simplifies equation (30) so that

$$\Gamma_{eq} = s_{11} + \frac{\Gamma_l}{1-\Gamma_l s_{22}} \qquad \textit{Equation 31}$$

Additionally, for small values of Γ_l and s_{22}, $\Gamma_l s_{22} \ll 1$, and equation (31) is further simplified as

$$\Gamma_{eq} \cong s_{11} + \Gamma_l \qquad \textit{Equation 32}$$

Generalizing for multiple discontinuities,

$$\Gamma_{eq} \cong \Gamma_l + \sum_{i=1}^{n} s_{11i} \qquad \textit{Equation 33}$$

where s_{11i} represents the i^{th} discontinuity. The real and imaginary parts of Γ_{eq} sum as follows:

$$\Gamma_{eq} \cong \Gamma_l + \sum_{i=1}^{n} s_{11i} = \Gamma_{l.re} + \sum_{i=1}^{n} s_{11.rei} + i\left[\Gamma_{l.im} + \sum_{i=1}^{n} s_{11.imi}\right] \qquad \textit{Equation 34}$$

Mullen and Pritchard [6] have demonstrated that, given a sufficient number of unrelated small discontinuities, the Central Limit Theorem applies to the characteristics of Γ_{eq}. Specifically, the real and imaginary components of Γ_{eq} will each tend towards a Gaussian distribution regardless of the distributions describing the discontinuities. The resulting distributions representing the real and imaginary components of Γ_{eq} both have a mean of zero and equal variance. Under these conditions, the distribution of magnitude, $\left|\Gamma_{eq}\right|$, is a Rayleigh distribution and has the probability density function

$$\mathrm{r}\left(x;\sigma\right)=\frac{x}{\sigma^2}\mathrm{e}^{-\frac{x^2}{2\sigma^2}} \qquad \textit{Equation 35}$$

where σ, is the Rayleigh distribution parameter. Note that σ, in this case, is the standard deviation of the Gaussian distributions describing the real and imaginary components of reflection coefficient. Therefore, if Γ_l and Γ_g are described by a Rayleigh distribution, then

$$u\left(\Gamma_{l.re}\right)=\sigma_l \qquad \textit{Equation 36}$$

$$u\left(\Gamma_{g.re}\right)=\sigma_g \qquad \textit{Equation 37}$$

The uncertainty of M, when relying on reflection coefficient magnitude described by a Rayleigh distribution is,

$$u\left(M\right)=2\sqrt{2}\sigma_l\sigma_g \qquad \textit{Equation 38}$$

A plot of the Rayleigh distribution is shown in Figure 6.

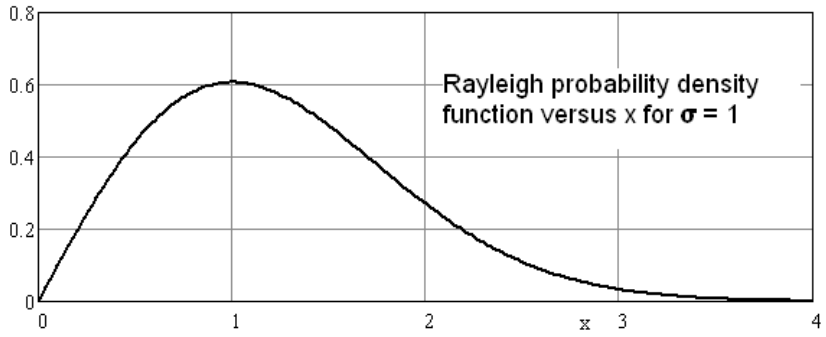

Figure 6. Rayleigh distribution.

Equation (34) led to the applicability of the Central Limit Theorem in this analysis. It also hints at the relative stability, or lack of significant drift, possible with reflection coefficient. Reflection coefficient is the sum effect of several physical discontinuities along a transmission path, the majority of which are likely not subject to significant physical stress. Components that are subject to physical stress, such as the mating surfaces of connectors, contribute only partly to the reflection coefficient. Therefore, through proper connector care (e.g., inspection, cleaning and replacement of worn or damaged surfaces), stable reflection coefficient is achievable.

6. Computing σ for the Rayleigh Distribution

To compute the σ parameter of the Rayleigh distribution, the authors would like to suggest using the 95th percentile of the distribution.

The Rayleigh cumulative distribution function (CDF) is the integral of the PDF, of course

$$\mathrm{R}(x) = 1 - \mathrm{e}^{-\frac{x^2}{2\sigma^2}} \qquad \textit{Equation 39}$$

The relationship between the 95th percentile value of the cumulative distribution function and the parameter σ can be found by solving

$$\mathrm{R}(x) = 0.95 = 1 - \mathrm{e}^{-\frac{x95^2}{2\sigma^2}} \qquad \textit{Equation 40}$$

Solving for σ gives

$$\sigma = \frac{x95}{\sqrt{2\ln(20)}} \qquad \textit{Equation 41}$$

Combining equations (38) and (41), the standard uncertainty of M, as related to the 95th percentile of the distribution of reflection coefficient magnitude, is

$$u(M) = \frac{\sqrt{2}}{\ln(20)}\Gamma 95_l \Gamma 95_g \qquad \textit{Equation 42}$$

In addition to estimating the σ parameter from the 95th percentile, other possibilities include the 99.73rd percentile, the 80th percentile, the mean, and the median of the distribution.

Table 1 shows the relationships between these population observations and σ, and the corresponding conversion to the 95th percentile for use with equation (42).

Γ Parameter	σ Computation	95th Percentile
Max (99.73rd percentile)	$\sigma = \frac{\Gamma max}{3.439}$	$\Gamma\ 95 = 0.712\Gamma\ max$
95th percentile	$\sigma = \frac{\Gamma 95}{\sqrt{2\ln(20)}}$	$\Gamma\ 95 = \Gamma\ 95$
80th percentile	$\sigma = \frac{\Gamma 80}{\sqrt{2\ln(5)}}$	$\Gamma\ 95 = 1.269\Gamma\ 80$
Mean	$\sigma = \Gamma mean\sqrt{2/\pi}$	$\Gamma\ 95 = 1.953\Gamma\ mean$
Median (50th percentile)	$\sigma = \frac{\Gamma median}{\sqrt{2\ln(2)}}$	$\Gamma\ 95 = 2.079\Gamma\ median$

Table 1. τ, σ and 95th percentile relationships for the Rayleigh distribution.

The first entry in Table 1 is labeled as "maximum", which is meant to address the scenario when reflection coefficient magnitude is expected to not exceed a given value. The "maximum" reflection coefficient magnitude cannot be mapped to a value of σ because the cumulative Rayleigh distribution never reaches 100%. A practice recommended by the authors is to assume that the "maximum" of this Rayleigh-distributed value is the equivalent of "3σ" for Gaussian-distributed random variables. The 3σ range is equivalent to a yield loss of 0.27%, or $\mathrm{CDF}(x) = 0.9973$. Solving this equation shows that $\sigma = xmax / 3.439$.

7. Another Distribution Combination

In some cases, the statistical distribution of one of the mismatches might be Rayleigh while the other relies on a measured magnitude value. Let Γ_1 represent the match of the Rayleigh-distributed element and $|\Gamma_2|$ for the measured mismatch element with a corresponding uncertainty. The standard uncertainty of M for that case is

$$u(M) = \sqrt{2}\frac{\Gamma 95_1}{\sqrt{\ln(20)}}\sqrt{|\Gamma_2|^2 + 2u^2(|\Gamma_2|)}$$

8. Summary of Distribution Equations for the Unknown Phase Case

Mismatch uncertainty has been computed for three realistic cases. Table 2 summarizes these equations for mismatch uncertainty. The first entry in Table 2 is most useful with the availability of measured values for reflection coefficient magnitude and corresponding standard uncertainties. The second entry is most useful for assumed values of reflection coefficient magnitude, for instance, when relying on data provided by the manufacturer across a wide range of frequencies. In this case, the Rayleigh distribution is an excellent model of reflection coefficient magnitude as the remaining sections of this paper demonstrate. The third entry in Table 2 addresses using both measured reflection coefficient values and assumed reflection coefficient values.

Condition	Standard uncertainty
Measured magnitude	$u(M)=\sqrt{2}\sqrt{\lvert\Gamma_l\rvert^2+2u^2\left(\lvert\Gamma_l\rvert\right)}\sqrt{\lvert\Gamma_g\rvert^2+2u^2\left(\lvert\Gamma_g\rvert\right)}$
Assumed Rayleigh	$u(M)=\frac{\sqrt{2}}{\ln(20)}\Gamma 95_l\Gamma 95_g$
Rayleigh/Measured combination	$u(M)=\sqrt{2}\frac{\Gamma 95_1}{\sqrt{\ln(20)}}\sqrt{\lvert\Gamma_2\rvert^2+2u^2\left(\lvert\Gamma_2\rvert\right)}$

Table 2. Summary of Recommended Standard Uncertainty Equations.

Common industry practice is to calculate mismatch uncertainty by the method described by Harris and Warner, which relies on the uncertainty having the U-shaped distribution, and is often used assuming reflection coefficient magnitudes are always at the maximum documented on a manufacturer's data sheet. To address the obvious overstatement of mismatch uncertainty in the latter case, an alternate practice is to assume uniformly distributed reflection coefficient values within a circle in the complex plane. Agilent Application Note 1449-3 [7] documents these practices; a companion calculator is available[8]. This application note refers to calculating mismatch uncertainty assuming uniformly distributed reflection coefficient as Case (a) and the Harris and Warner model as Case (b). Table 3 lists the equations used for these calculations for reference. The authors recommend using the Table 2 equations for determining mismatch uncertainty when reflection coefficient phase is not known.

Distribution	Standard uncertainty
Harris and warner (1449-3 case (b))	$u(M)=\sqrt{2}\lvert\Gamma_l\rvert\lvert\Gamma_g\rvert$
Uniform (1449-3 case (a))	$u(M)=\frac{\sqrt{2}}{2}\lvert\Gamma_l\rvert\lvert\Gamma_g\rvert$

Table 3. Standard Uncertainty Equations Used in Common Models.

The first entry in Table 2 is a generalized solution for the Harris and Warner model (the first entry in Table 3). It accounts for the error associated with measured values of reflection coefficient magnitude as well as the error due to unknown phase. When it is necessary to assume reflection coefficient magnitude values, the Rayleigh distribution gives the most accurate estimate of uncertainty, particularly when compared to the uniform distribution.

9. Estimating the Rayleigh Distribution Parameter from Manufacturer Data

Manufacturers give us information on the distribution of reflection coefficient magnitude in many different ways. Agilent Technologies provides examples in the fields of power sensors, signal sources and signal analyzers.

For power sensors, Agilent gives a warranted specification on *VSWR*. In some more modern power sensors, Agilent also gives a graph of the typical *VSWR* versus frequency.

The authors have analyzed statistical data on the 8481A (not the more modern N8481A). Some specifications for *VSWR* for this device are given in Table 4.

Frequency	Maximum *VSWR*
50 MHz to 2 GHz	1.10
2 to 12.4 GHz	1.18
12.4 to 18 GHz	1.28

Table 4. Specifications for 8481A power sensor.

Figure 7 shows the maximum specification, in terms of reflection coefficient magnitude and the mean values as a function of frequency determined from the statistical data.

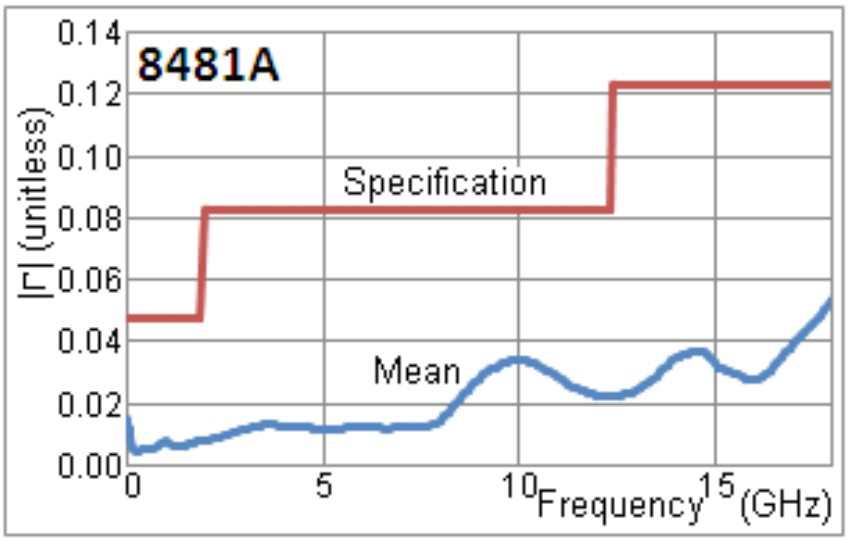

Figure 7. Specified and mean observed reflection coefficient magnitude, $|\Gamma|$, for 8481A power sensor.

Consider this example of an estimate of $\Gamma 95$ from Γ max for the 8481A power sensor in the range 0 to 8 GHz:

$$VSWRmax = 1.18 \qquad \textit{Equation 43}$$

$$\Gamma \max = \frac{VSWRmax - 1}{VSWRmax + 1} = 0.0826 \qquad \textit{Equation 44}$$

$$\Gamma 95 = 0.712 \Gamma max = 0.0588 \qquad \textit{Equation 45}$$

Consider this example of the estimation of $\Gamma 95$ from mean for the 8481A power sensor in the range 0 to 8 GHz:

$$\Gamma mean = 0.014 \qquad \textit{Equation 46}$$

$$\Gamma 95 = 1.953 \Gamma mean = 0.0273 \qquad \textit{Equation 47}$$

These two ways of estimating yield results that differ by more than a factor of two. The latter, coming as it does from real observations instead of data sheets, is the more accurate. The observed $\Gamma 95$ is 0.0219.

Therefore, the assumption that the data sheet "maximum" is the equivalent of the 3σ range overstates the uncertainty by a factor of two in this case. It is still a good way to minimize the risk of understating the uncertainty when no other information is available.

Next, consider a signal analyzer. The Agilent PXA gives the plot in Figure 8 of *VSWR* for three sample instruments in high band (3.5 to 26.5 GHz) with the preamp on, with 0 dB attenuation:

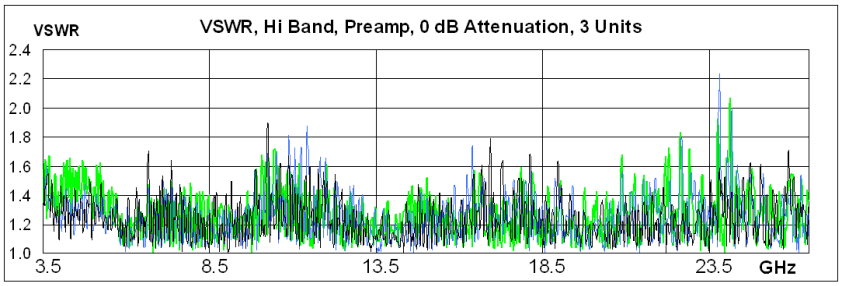

Figure 8. An example signal analyzer VSWR plot.

One can estimate by eye the level that is exceeded by 5% of the frequency points. That might be *VSWR* = 1.6, thus $\Gamma 95$ = 0.23. (A numeric observation from this data set gave *VSWR* = 1.52.)

Finally, consider a signal generator, such as the Agilent N5183A. This device has a stated *VSWR* of 1.6 (typ) for frequencies up to 20 GHz. The stated definition of (typ) for this product line is that level which is surpassed by 80% of the instruments at the worst frequency in the range. Treating this as an 80th percentile for all frequencies, an assumption which obviously leads to overstatement of the uncertainty, compute $\Gamma 80$ = 0.231 and thus $\Gamma 95$ = 0.293. Actual data shows this estimate to give a highly overstated uncertainty; the observed $\Gamma 95$ = 0.140.

To summarize this section: The 95th percentile for reflection coefficient magnitude can be computed from data sheet specifications such as the maximum VSWR or the 80th percentile *VSWR*, or from typical graphs. Results from data sheets are often overstated by a factor of two; results from typical graphs are closer to reality.

10. Comparing Observed Distributions to the Rayleigh Distribution

How close is the Rayleigh model to reality? Again, the authors have investigated examples of the most commonly used metrology elements of their experience: power sensors, signal generators and signal analyzers. The answer is "very close" in all cases.

Power sensors are the simplest of these elements. Because the Rayleigh model seemingly depends on a large number of reflective elements and the central limit theorem, we might expect the power sensors to not be a particularly good fit to a Rayleigh distribution. But they are. Figure 9 compares the measured reflection coefficient magnitude, $|\Gamma|$, with a best-fit model in the 0 to 8 GHz and 12.4 to 18 GHz regions.

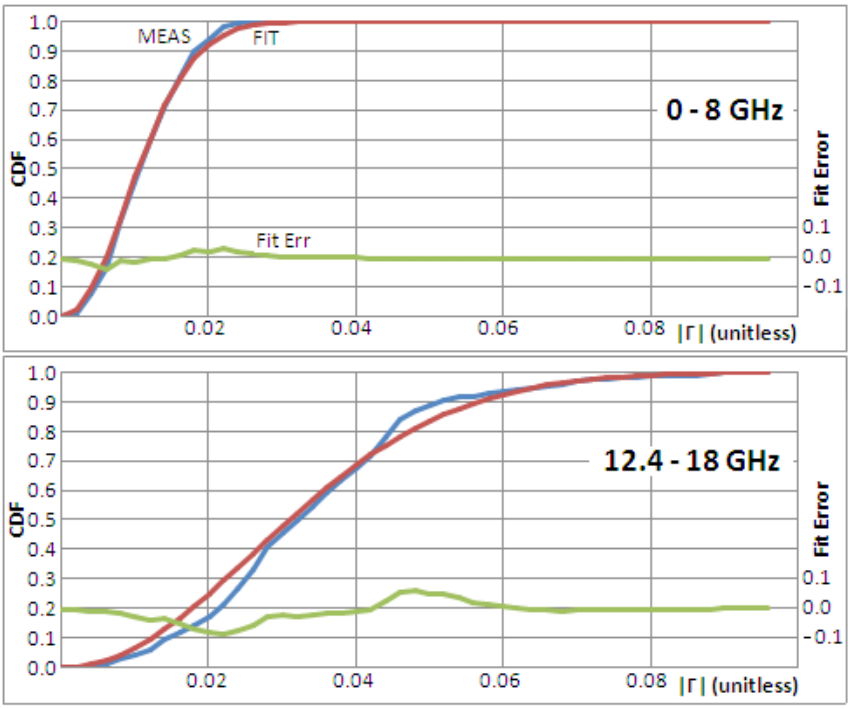

Figure 9. Cumulative distribution functions for 8481A power sensors in two frequency ranges.

The fit in the 0 to 8 GHz region is remarkably good. Even in the higher frequency plot, where some amount of chaos is implied by the variation in the mean *VSWR* (see Figure 7), the fit shows the general characteristic of the Rayleigh model.

Next, consider a signal generator. For the N5183A, 0 to 20 GHz, see Figure 10.

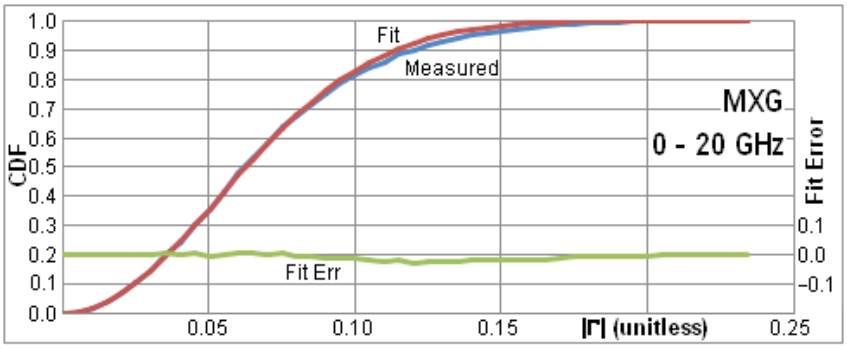

Figure 10. Cumulative distribution functions for N5183 signal source, 0 to 20 GHz.

The 80th percentile performance specified for this model is a *VSWR* of 1.6:1, which is a $|\Gamma|$ of 0.23. The figure shows that the 80th percentile at all frequencies is a $|\Gamma|$ of 0.09. The use of an 80th percentile performance statistic for the worst frequency results in mismatch uncertainty estimates that are a factor of more than two higher than they would be if the 80th percentile statement were based on all frequencies.

Finally, consider the PXA signal/spectrum analyzer. Figure 11 shows the behavior of the high-band preamplifier with 0 dB input attenuation.

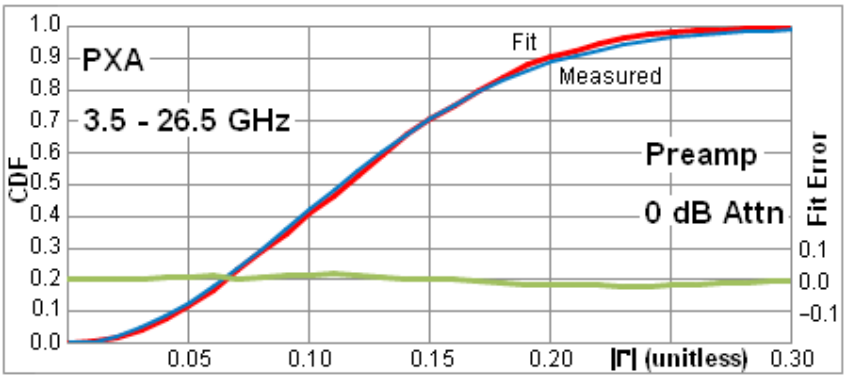

Figure 11. Cumulative distribution functions for PXA signal analyzer, 3.5 to 26.5 GHz, preamp, 0 dB attenuation.

Again, an excellent fit to a Rayleigh model. Analysis of low band (0 to 3.6 GHz) with 10 dB attenuation shows similarly excellent fit, with $|\Gamma 95|$ = 0.064.

In summary, power sensors, signal sources and signal analyzers all have reflection coefficients that are very well modeled as having a Rayleigh probability density function.

11. Bivariate Gaussian Distribution

The Rayleigh distribution is theoretically possible even without the other part of the hypothesis: that the real and imaginary components of the reflections are independently of Gaussian distribution. The distribution is of interest to some researchers in the field. Some frequency ranges of spectrum analyzers and power sensors were inspected for Gaussian behavior of the real and imaginary parts. There has been no substantial deviation from that behavior. Figure 12 shows a test of the Gaussian hypothesis for a spectrum analyzer over the frequency range of 0 to 3.6 GHz, with 10 dB input attenuation. The reflections were derotated to minimize the spinning of the phase across this frequency range. The distributions of both quadrature components, and 45° rotated versions of them, were all inspected. These were judged for conformance with a Gaussian distribution by computing R^2, the coefficient of determination, of the mapping of the cumulative distribution function to that of an ideal Gaussian. R^2 values ranged from 99.3 to 99.8%, which represents a good match to a Gaussian model. In Figure 12, the straight line represents an ideal Gaussian model. The actual curve agrees very well, especially in the region of 1 to 99% cumulative probability.

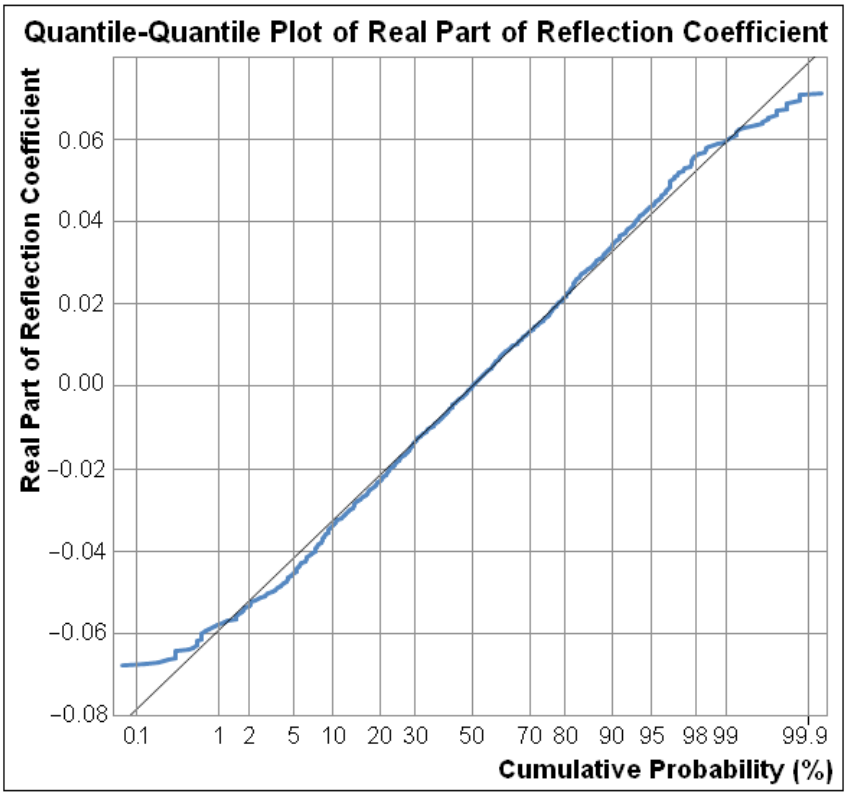

Figure 12. Normal probability plot of spectrum analyzer input reflection, 0 to 3.6 GHz, 10 dB attenuation.

12. Comparing Estimation Quality for Rayleigh and Other Distributions

Let us discuss the extent of the errors from using different models for the distribution.

To judge how large the fit errors are, consider that the very frequently used model for mismatch uncertainty is the **U**-shaped distribution (see the left side of Figure 4), which is equivalent to a known, maximum $|\Gamma|$ with uniformly distributed phase. For the 8481A, 12.4 to 18 GHz example (Table 4), that would be a *VSWR* of 1.28:1, thus a $|\Gamma|$ of 0.123. By comparison, the observed statistical distribution of $|\Gamma|$ (Figure 9, lower) shows no probability of $|\Gamma|$ higher than 0.090, and only minor variations from a perfectly Rayleigh model with $|\Gamma|$ between 0.01 and 0.08. The Rayleigh model is dramatically more accurate, even at its worst, than using the textual data sheet specification.

Figure 13 shows a plot of the CDF versus $|\Gamma|$ for the models documented for use in estimating amplitude uncertainty. The CDFs are discussed here to help with understanding the effect of model choice on the accuracy of estimating the uncertainty.

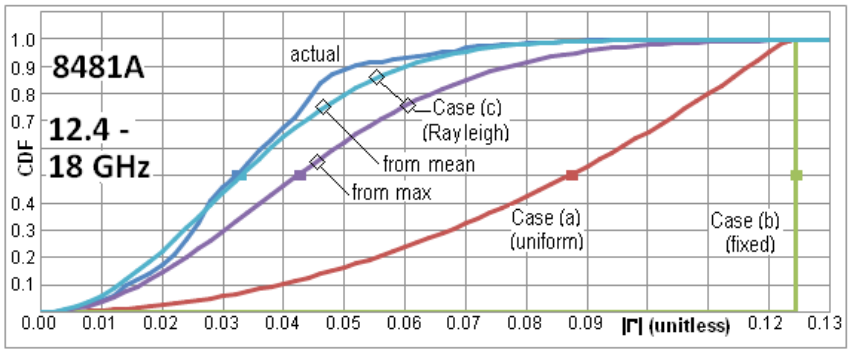

Figure 13. Cumulative distribution functions for $|\Gamma|$.

Markers are shown on each curve at the point of 50th percentile cumulative probability. In other words, the square markers show the medians of the distributions. The graph shows median values for $|\Gamma|$ from actual measurement data, estimates assuming Rayleigh distributions and estimates using common industry practices for determining mismatch uncertainty.

The curve at the bottom right is the most conservative, leading to the most extreme overstatement of uncertainty. This is the CDF assuming that the magnitude of the reflection coefficient is always at its data sheet maximum, that is, Case (b) from Agilent Application Note 1449-3, the model that gives the **U**-shaped distribution of mismatch uncertainty. This curve shows that the $|\Gamma|$ is always 0.123. The next curve is the Case (a) model CDF from that application note; it assumes equally probable $|\Gamma|$ anywhere within a circle in the complex plane. The median value of the $|\Gamma|$ is smaller than in the first case by 30%.

A rough approximation is that the mismatch uncertainty is proportional to the median of the distributions. By this rough approximation, case (a) gives a lower estimate of mismatch uncertainty than case b by 30%.

Looking at the CDF curve in more detail, it can be seen that in half of all cases, the uncertainty is at least 30% smaller than with the Case (b) model. In 10% of observations, the $|\Gamma|$ is only 0.04 or less, substantially less than in the Case (b) example. There is no accumulated probability (y axis) for which the case (a) model shows higher $|\Gamma|$. Overall, this model gives a lower computed standard uncertainty by a factor of two.

The next curve, labeled "Case (c)" and "from max," is based on the Rayleigh distribution, assuming that the data sheet maximum $|\Gamma|$ corresponds to "3σ" yield loss. A rough approximation that the uncertainty is proportional to the median $|\Gamma|$ predicts that "case (c) from max" shows less than half the error of case (a). It shows even lower median $|\Gamma|$, or $|\Gamma|$ at any cumulative probability short of very near to 100%.

The next curve ("from mean") is also based on the Rayleigh distribution, using the observed mean reflection coefficient to compute the model parameter. Finally, the curve with the leftmost median is actual $|\Gamma|$. It results in similar uncertainty to the least conservative of the modeling techniques.

To review, consider again the concept that the estimated uncertainty is roughly proportional to the median of the distribution function. By this analysis, it is obvious that Rayleigh model for distribution, using the mean $|\Gamma|$ to estimate the Rayleigh parameter, gives the best approximation to reality, as well as the lowest uncertainty of any of the models.

13. Considering the Rayleigh Distribution in Narrow Frequency Ranges

The analysis presented thus far has been for wide frequency range data. The *VSWR* plot presented earlier for the three PXA units (Figure 8) shows us that there is repeatable character to the reflections. If usage is over a narrower range of frequencies, the estimation of uncertainty can be accomplished with different techniques. For example, in that plot, *VSWR* around 13.5 GHz is particularly low, while that near 24 GHz is particularly high. When estimating amplitude uncertainty in a narrow and atypical frequency region, the Rayleigh model may not work well.

Figure 14 shows observations of the mean and standard deviation of $|\Gamma|$ for the MXG signal source across 20 GHz, from the observation of 13 prototype instruments. If a metrologist knows this characteristic and is working in a narrowband range, the Rayleigh model is not critical to reducing the overstatement of the mismatch uncertainty.

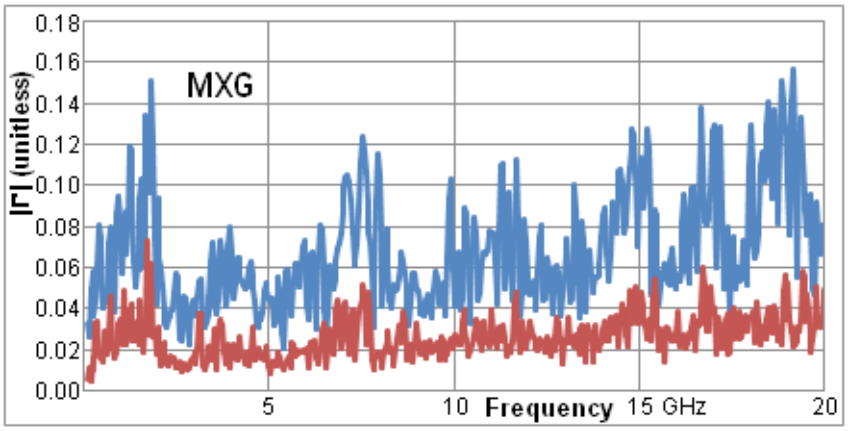

Figure 14. Mean (upper line) and σ (lower line) of $|\Gamma|$ versus frequency for a group of signal generators of the same instrument model.

Notice, here, how the standard deviation scales with the average $|\Gamma|$. The ratio of these two parameters is that the standard deviation is, on average, 41% of the mean for this data set. Figure 15 shows a scattergram of the mean on the horizontal axis and the standard deviation on the vertical axis. The 41% ratio can be seen in the trend line.

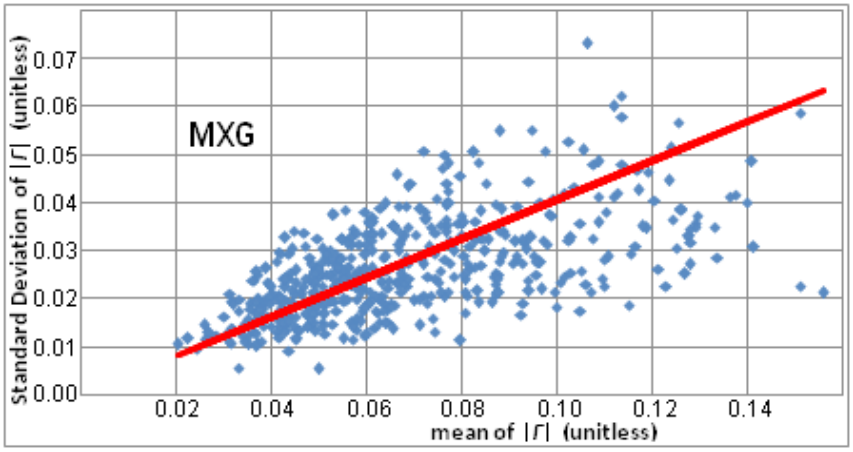

Figure 15. Scattergram of mean vs. σ of $|\Gamma|$ for a signal generator.

If the statistical distribution of $|\Gamma|$ versus the population of instruments had been Rayleigh, we would expect the ratio of standard deviation to mean to be 52%. Thus, the statistical distribution is not quite Rayleigh versus instruments at any particular frequency; it is only Rayleigh-distributed across a wide range of frequencies.

Figure 16 shows a Monte Carlo simulation of this scattergram for an ideal Rayleigh distribution at each frequency point with the same number of sample points (13), and the same distribution of the mean of $|\Gamma|$. Overall, It looks very similar to the previous figure after modest vertical rescaling. (There is an exception at high levels of $|\Gamma|$. This implies that, at those frequencies where the reflections are particularly strong, they are more repeatable across the instrument population.) The similarity supports the conclusion that the distribution of $|\Gamma|$ versus the population of instruments is close to Rayleigh even in the narrowband case.

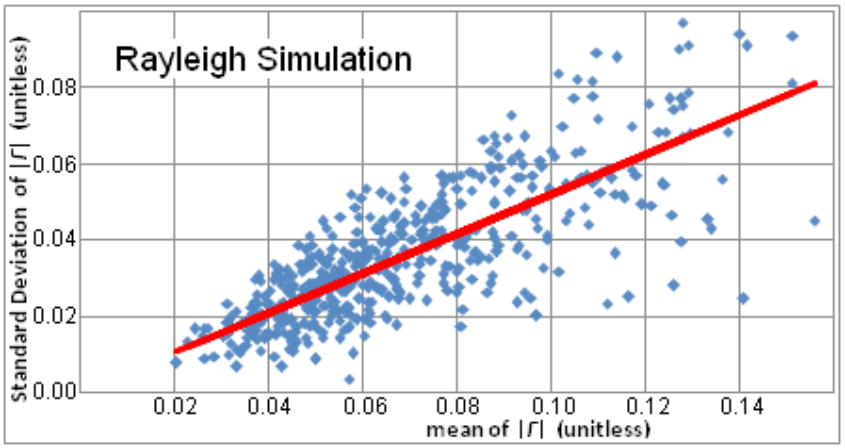

Figure 16. Scattergram of mean vs. σ of $|\Gamma|$ from Monte Carlo simulation with ideal Rayleigh distribution.

Of course, if the $|\Gamma|$ were perfectly consistent at any frequency across the population of instruments, its standard deviation would be 0% of its mean. At a 41% observed ratio versus the ideal 52% of Rayleigh statistics, the distribution is much closer to Rayleigh than to a constant. The degree to which the statistical distribution includes, or is dominated by, repeatable elements in a measuring device cannot be generalized. Analysis of this case has shown that treating the statistical distribution as Rayleigh will overestimate the measurement uncertainty by about 5% at most narrowband frequencies. That would still be a big improvement over using other models of the statistical distribution.

Analysis of the 8481A power sensor showed a standard deviation of $|\Gamma|$ of 38% of its mean, on average, across frequencies, and a similarly minor overestimation of uncertainty with the Rayleigh model.

Finally, theoretical analysis shows that treating a $|\Gamma|$ as being Rayleigh-distributed with a known mean, when it is actually constant, will cause a modest overestimation of the measurement uncertainty by a factor of $\sqrt{(4/\pi)}$, thus about 13% higher. Thus, using the Rayleigh model with an observed mean leads to quite modest overestimation of measurement uncertainty, while other models can lead to much greater overestimations. The Rayleigh model should therefore be the default model, even for narrow band situations.

14. Summary of Recommended Practices

This paper has shown how errors arise due to multiple reflections in RF and microwave systems. When the reflection coefficient is known, both magnitude and phase, it is possible to correct for mismatch with known uncertainty. However, as is common, when phase is not known, determining mismatch uncertainty requires a different model. Three such models are available. One well suited for determining mismatch uncertainty using measured values of reflection coefficient magnitude, another relying on Rayleigh distributed values when reflection coefficient magnitude must be assumed, and the third combining measured and assumed values. Equations for these cases are summarized in Table 2.

For the common case where reflection coefficient magnitude must be assumed from data provided by the manufacturer across a wide range of frequencies, this paper has shown that the Rayleigh model is, in all of many cases investigated, an excellent model of the distribution. The metrologist is then faced with finding the parameter of the Rayleigh distribution, such as its 95th percentile. In some cases, this can be computed from the mean; in others, from visual inspection of a graph. If the only information known is a "maximum," that can be treated as the 99.73rd percentile and used to compute the 95th percentile. In the case of knowing the 80th percentile at the worst frequency, the 95th percentile parameter can be computed from that, but the result is usually very conservative, by more than a factor of two in the example studied, though this is still much more accurate than treating the 80th percentile as a constant reflection coefficient magnitude.

Overall, treating reflection coefficient magnitude as Rayleigh-distributed leads to substantially more accurate, yet still conservative, estimates of standard uncertainty due to mismatch, compared to the methods commonly used. The Rayleigh-based process will usually give a six times lower estimate of uncertainty than the most popular method using the **U**-shaped distribution that assumes a constant reflection coefficient magnitude with random phase.

Acknowledgement

The authors would like to acknowledge Dr. Blair Hall for his critical and helpful review of this work.

References

[1] Guide to the Expression of Uncertainty in Measurement (GUM), BIPM, IEC, IFCC, ISO, IUPAC, IUPAP, OIML – ISO, Geneva, Switzerland, 1995.

[2] Ridler, N. M. and Salter, H. J., An approach to the treatment of uncertainty in complex S-parameter measurements, 2002, Metrologia 39 295-302.

[3] Hall, B. D., On the expression of measurement uncertainty for complex quantities with unknown phase, 2011, Metrologia 48 324–332.

[4] Hall, B.D., Some considerations related to the evaluation of measurement uncertainty for complex-valued quantities in radio frequency measurements, 2007, Metrologia, 44 L62-L67.

[5] Harris, I. A. and Warner, F. L., Re-examination of mismatch uncertainty when measuring microwave power and attenuation, Microwaves, Optics and Antennas, IEE Proceedings ~ H, February 1981, Volume 128, Issue 1.

[6] Mullen, J. A. and Pritchard, W. L., The Statistical Prediction of Voltage Standing-Wave Ratio, Microwave Theory and Techniques, IRE Transactions, April 1957, Volume 5, Issue 2.

[7] Fundamentals of RF and Microwave Power Measurements (Part 3) Power Measurement Uncertainty per International Guides. Agilent Application Note AN 1449-3, April 5, 2011, literature number 5988-9215EN. Available on-line.

[8] Average Power Sensor Uncertainty Calculator. Agilent Technologies, April 6, 2011. Available on-line.

Appendix A

Often, reflection coefficient uncertainties are given in polar form. To convert reflection coefficient uncertainties from polar form to rectangular form is to transform from one coordinate system to another. It is convenient to do this in matrix form. Given a quantity in polar form as $X=(M,\Theta)$ the rectangular form is $Y=(R,I)$, where $R=(M\cos\Theta)$, $I=(M\sin\Theta)$, and Θ is in radians. Unfortunately, reflection coefficient uncertainties in polar form are not Gaussian and the transformation to rectangular coordinates is nonlinear for magnitude values near the origin. Therefore, the propagation of uncertainties is only valid when $u(M)\ll M$. The propagation of uncertainty is given by Ridler and Salter [2] and Hall [4].

$$v(Y)=Jv(X)J^T \qquad \textit{Equation 48}$$

where $v(X)$ and $v(Y)$ are the covariance matrices of X and Y, and J is the Jacobian matrix of the transform from X to Y. The covariance matrices are,

$$v(Y)=\begin{bmatrix} u^2(R) & u(R,I) \\ u(I,R) & u^2(I) \end{bmatrix} \qquad \textit{Equation 49}$$

$$v(X)=\begin{bmatrix} u^2(M) & u(M,\Theta) \\ u(\Theta,M) & u^2(\Theta) \end{bmatrix} \qquad \textit{Equation 50}$$

where the diagonal elements of the covariance matrices represent the square of the standard uncertainty of the corresponding terms and the off-diagonal elements represent the covariance between the corresponding terms. The Jacobian matrix gives the sensitivity coefficients of the transform. In this case, letting $f_1(M,\Theta)=(M\cos\Theta)$ and $f_2(M,\Theta)=(M\sin\Theta)$, then

$$J=\begin{bmatrix} \frac{\partial f_1}{\partial M} & \frac{\partial f_1}{\partial \Theta} \\ \frac{\partial f_2}{\partial M} & \frac{\partial f_2}{\partial \Theta} \end{bmatrix}=\begin{bmatrix} \cos\Theta & -M\sin\Theta \\ \sin\Theta & M\cos\Theta \end{bmatrix} \qquad \textit{Equation 51}$$

To transform reflection coefficient uncertainties to rectangular form, the covariance matrix therefore, is

$$\begin{bmatrix} u^2(R) & u(R,I) \\ u(I,R) & u^2(I) \end{bmatrix}=\begin{bmatrix} \cos\Theta & -M\sin\Theta \\ \sin\Theta & M\cos\Theta \end{bmatrix}\bullet\begin{bmatrix} u^2(M) & u(M,\Theta) \\ u(\Theta,M) & u^2(\Theta) \end{bmatrix}\bullet\begin{bmatrix} \cos\Theta & \sin\Theta \\ -M\sin\Theta & M\cos\Theta \end{bmatrix} \qquad \textit{Equation 52}$$

where matrix multiplication has the form

$$\begin{bmatrix} a & b \\ c & d \end{bmatrix} \bullet \begin{bmatrix} e & f \\ g & h \end{bmatrix} = \begin{bmatrix} ae+bg & af+bh \\ ce+dg & cf+dh \end{bmatrix} \qquad \textit{Equation 53}$$

A common practice when reporting reflection coefficient uncertainties in polar form, is that the phase uncertainty derives from the magnitude uncertainty using an assumption of a circular uncertainty region and stating the phase uncertainty as $u(\Theta) = \arcsin\left(\frac{u(M)}{M}\right)$. The covariance matrix, in polar form in this case, is

$$\begin{bmatrix} u^2(M) & 0 \\ 0 & u^2(\Theta) \end{bmatrix} \qquad \textit{Equation 54}$$

where the off-diagonal covariance terms are zero. After the transformation, using equation (49) and equation (52), the covariance matrix, in rectangular form in this case, is

$$\begin{bmatrix} u^2(R) & 0 \\ 0 & u^2(I) \end{bmatrix} \qquad \textit{Equation 55}$$

where $u^2(M) \cong u^2(R) \cong u^2(I)$

Agilent Email Updates

www.agilent.com/find/emailupdates
Get the latest information on the products and applications you select.

LXI

www.lxistandard.org
LAN eXtensions for Instruments puts the power of Ethernet and the Web inside your test systems. Agilent is a founding member of the LXI consortium.

Agilent Channel Partners

www.agilent.com/find/channelpartners
Get the best of both worlds: Agilent's measurement expertise and product breadth, combined with channel partner convenience.

Agilent Advantage Services

Agilent Advantage Services is committed to your success throughout your equipment's lifetime. To keep you competitive, we continually invest in tools and processes that speed up calibration and repair and reduce your cost of ownership. You can also use Infoline Web Services to manage equipment and services more effectively. By sharing our measurement and service expertise, we help you create the products that change our world.

www.agilent.com/find/advantageservices

Agilent Electronic Measurement Group
DEKRA Certified
ISO 9001:2008
Quality Management System

www.agilent.com/quality

For more information on Agilent Technologies' products, applications or services, please contact your local Agilent office. The complete list is available at:

www.agilent.com/find/contactus

Americas	
Canada	(877) 894 4414
Brazil	(11) 4197 3500
Mexico	01800 5064 800
United States	(800) 829 4444

Asia Pacific	
Australia	1 800 629 485
China	800 810 0189
Hong Kong	800 938 693
India	1 800 112 929
Japan	0120 (421) 345
Korea	080 769 0800
Malaysia	1 800 888 848
Singapore	1 800 375 8100
Taiwan	0800 047 866
Other AP Countries	(65) 375 8100

Europe & Middle East	
Belgium	32 (0) 2 404 93 40
Denmark	45 70 13 15 15
Finland	358 (0) 10 855 2100
France	0825 010 700*
	*0.125 €/minute
Germany	49 (0) 7031 464 6333
Ireland	1890 924 204
Israel	972-3-9288-504/544
Italy	39 02 92 60 8484
Netherlands	31 (0) 20 547 2111
Spain	34 (91) 631 3300
Sweden	0200-88 22 55
United Kingdom	44 (0) 131 452 0200

For other unlisted countries:
www.agilent.com/find/contactus

Revised: June 8, 2011

Product specifications and descriptions in this document subject to change without notice.

Published in USA, October 6, 2011
5990-9185EN

Agilent Technologies